Journal of X-Ray Science and Technology 20 (2012) 277–289
DOI 10.3233/XST-2012-0337
IOS Press

TV-Based image reconstruction of multiple objects in a fixed source-detector geometry

Yang Lu[a], Zhenyu Yang[a], Jun Zhao[a,*] and Ge Wang[b]
[a]*School of Biomedical Engineering, Shanghai Jiao Tong University, Shanghai, China*
[b]*Biomedical Imaging Division, VT-WFU School of Biomedical Engineering and Science, Blacksburg, VA, USA*

Received 1 September 2011
Revised 23 April 2012
Accepted 15 May 2012

Abstract. In this paper, we study how to reconstruct multiple objects tomographically from their overlapped x-ray projections. We propose a new rotation-translation scanning mode for a fixed source-detector geometry, in which the objects are individually translated periodically while they are rotated during the data acquisition. The reconstruction scheme performs SART reconstruction and TV minimization alternatingly. The scanning parameters are evaluated in a series of numerical experiments. Promising results are obtained in the cases of two and four objects respectively. The major advantage of our approach is that the scanning time can be reduced by about 46% (for two objects) and 67% (for four objects) respectively, improving the imaging facility throughput significantly.

Keywords: Computed tomography (CT), total variation (TV) minimization, image reconstruction, multiple objects

1. Introduction

Computed tomography (CT) has been widely used as an important non-destructive imaging technique in hospitals, clinics, and laboratories since its emergence in 1970s. In the clinical applications, it is required to rotate the x-ray source and the detector assembly simultaneously while keeping the patient table stable (for example, to image an organ) or in motion (such as for whole body imaging). In contrast to such a rotated source-detector geometry, in micro-CT scanners we often employ a fixed source-detector geometry [1,2], and in a synchrotron CT system the fixed source-detector geometry is a must because it is impossible to rotate the x-ray source. From the mathematical point of view, the motion of the source and detector assembly can be equally expressed as the object's motion. The object is placed on a sample stage which is controlled by one or several motors for translation and rotation. Although such a fixed source-detector geometry reduces mechanical complexity, the scanning speed is rather slow. Since the experimental time slot is especially precious for synchrotron CT facilities, researchers may have to wait for a long period for their experiments.

*Corresponding author: Jun Zhao, School of Biomedical Engineering, Shanghai Jiao Tong University, Shanghai 200240, China. E-mail: junzhao@sjtuedu.cn.

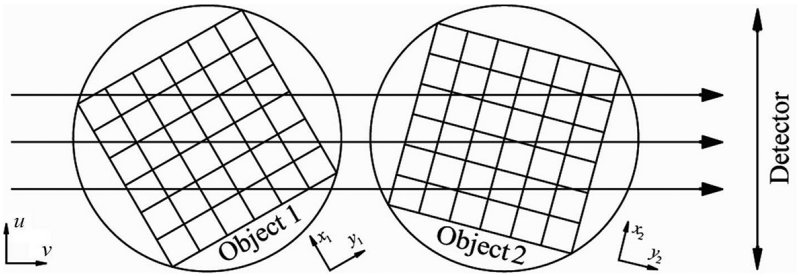

Fig. 1. Imaging model for two objects in a fixed source-detector geometry.

In the area of computed tomography, scanning time is equivalent to the number of projections in some sense. In order to reduce the time, one direct method is to reduce the number of projections. Notice that the x-ray from a synchrotron beamline is of high intensity. It remains high flux after passing through one or more samples. Hence, it is feasible to scan multiple objects simultaneously using the synchrotron radiation, thus reducing the data acquisition time.

On the other hand it has been demonstrated that by minimizing the l_1 norm of a sparsified image, or more specifically the total variation (TV) of the image, it is possible to reconstruct the image satisfactorily from few projections [3–6]. The idea of minimizing the l_1 norm of a sparsified image comes from compressive sensing, which is being developed rapidly over the past years [7,8] and applied to almost all the fields of engineering [3,9–12]. The main result of compressive sensing is that even from few random measurements it can accurately estimate the correct signal by minimizing the l_1 norm of the signal. The sparseness of the signal is crucial in the application of compressive sensing. As a two dimensional signal, an image itself may not have many zero pixels but its sparsifying transform such as its gradient image has.

In this paper, we studied on the image reconstruction from overlapped projections of multiple objects in a fixed source-detector geometry. The rest of this paper is organized as follows. In Section 2, we describe the imaging model, the rotation-translation mode and the SART-TV algorithm. In Section 3, the numerical results of reconstructions of two objects and four objects are presented. In Section 4, we discuss the related issues and conclude the paper.

2. Method

2.1. Imaging model

As illustrated in Fig. 1, an x-ray source and a detector array are fixed on the table, and multiple objects on the sample stages are placed between them. In this work, we focus on 2D image reconstruction with parallel beam CT so that the projection can be described as a line integral through the continuous objects

$$p(u) = \sum_{i=1}^{N_o} \int\limits_{(x_i,y_i)\in ray} f_i(x_i, y_i)\mathrm{d}y, \tag{1}$$

where $f_i(x_i, y_i)$ represents the i^{th} object in a local coordinate system (x_i, y_i), N_o the number of the objects, and $p(u)$ is the projection received by the one dimensional detector at location u.

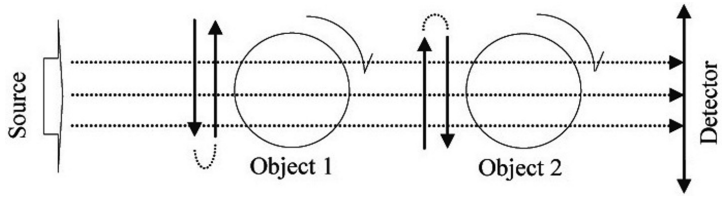

Fig. 2. Illustration of rotation-translation mode in the case of two objects. Both objects are rotated at a uniform speed and their centers are switched between two positions.

The detector array is considered as straight with equally spaced bins. Each bin receives a single ray through the objects, and this measurement can be discretized as

$$\overrightarrow{p} = \sum_{i=1}^{N_o} M_i \overrightarrow{f_i}, \tag{2}$$

where the vector $\overrightarrow{p}$ of length N_b represents the measured projection, the vector $\overrightarrow{f_i}$ of length $W_1 \cdot W_2$ is an image to be reconstructed, the index k of element $\overrightarrow{f_i}(k)$ can be related to the 2D image matrix $f_i(m_1, m_2)$ as

$$k = (m_1 - 1)W_2 + m_2, \quad m_1 = 1, \ldots, W_1,\ m_2 = 1, \ldots, W_2, \tag{3}$$

where (m_1, m_2) indicate the element locations, integers W_1 and W_2 are the width and height of the image array respectively, and the system matrix M_i approximates the integral coefficients of the corresponding object function. We utilize the ray-driven projection model [13] where the system matrix weights $M_i^{j,k}$ are computed by calculating the intersection length of the j^{th} ray through the k^{th} pixel of the i^{th} image. A detailed description of the system matrix M_i can be found in [4].

2.2. Problem statement

Assuming that objects are piece-wise constant, then the goal of our problem is to find $\vec{f_i}$ from $\vec{p}$, which is the solution of

$$\min \sum_{i=1}^{N_o} \|\vec{f_i}\|_{TV} \quad \text{subject to} \quad \vec{p} = \sum_{i=1}^{N_o} M_i \vec{f_i} \text{ and } \vec{f_i} \geqslant 0 \tag{4}$$

To solve this problem, first let us consider a typical case. Suppose multiple objects are rotated at the same speed and along the same direction (clockwise or counter-clockwise). Thus, the system matrix $M_i(i = 1, 2, \ldots, N_o)$ for each object is identical. Then, the aforementioned problem becomes a linear system equation

$$\overrightarrow{p} = M \left(\sum_{i=1}^{N_o} \overrightarrow{f_i} \right), \tag{5}$$

where M represents the identical system matrixes $M_i(i = 1, 2, \ldots, N_o)$. The summed part $\sum_{i=1}^{N_o} \vec{f_i}$ is equivalent to a new single vector $\vec{f}$, and every $\vec{f_i}$ can be set to $\frac{\vec{f}}{N_o}$ after the reconstruction. That is, the

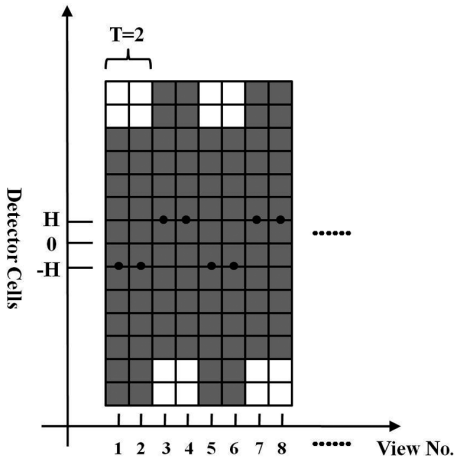

Fig. 3. Sinogram of a single object according to Eq. (6). The gray blocks correspond to the detector bins which record projection signals, and the white blocks correspond to those do not record signals. The black dots show the centers of projections.

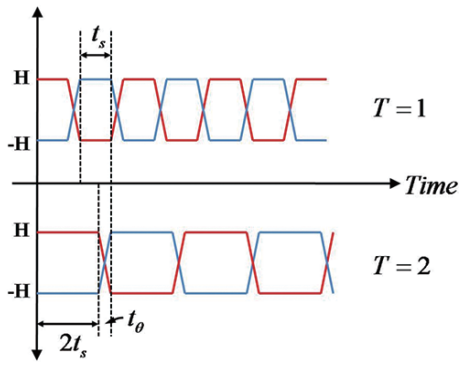

Fig. 4. Illustration of t_θ and t_s. The red lines and the blue lines are the center positions of different objects, respectively. The objects change their positions after acquisition of one sinogram when $T = 1$, and after acquisition of two sinograms when $T = 2$. (Colours are visible in the online version of the article; http://dx.doi.org/10.3233/XST-2012-0337)

identical images are produced as the average of the original individual images. Another case is that two objects are rotated at the same speed but along the opposite directions. Considering the mirror image of an object, we find that it has the same rotation speed and is rotated along the opposite direction. Hence, the reconstructed image will be the average of one object and the mirror image of the other object.

2.3. Translation modulated projections

Reconstructions from the overlapped projections were studied by Yang et al. [6] and Yu et al. [14]. In their studies, distributed sources were used to scan one object simultaneously, and all the projections were received by one detector. Clearly, such projections were partially overlapped. Their results showed the possibilities of accurate reconstructions from those overlapped projections. However, their studies focused on one object. Their strategy is to use a simplified system matrix. In our application, the difficulties are not only the overlapped projections but also the identical system matrixes. The identity of the system matrixes makes the objects at different positions logically equivalent. Specifically, what they did is to reconstruct an image from redundant information while we are trying to reconstruct images from incomplete information. As discussed previously, without priori knowledge, this problem can not be solved. Since the overlapped projections and the identical system matrixes are two main obstacles, we may find the solution if at least one of them is cleared. In this section, we will propose a new scanning mode, solving the problem from the system matrix perspective.

The system matrixes are determined by the scanning geometry and the motion of objects. Typically, in a fixed source-detector geometry the object's motion means rotation. Our idea is the object's motion should consist of rotation and translation along the direction perpendicular to the x-ray beams, see Fig. 2. The loci of the object center points can be described as

$$u_i = \frac{2H}{N_o - 1} \bmod \left(\left\lceil \frac{n}{T} \right\rceil + i, N_o \right) - H \tag{6}$$

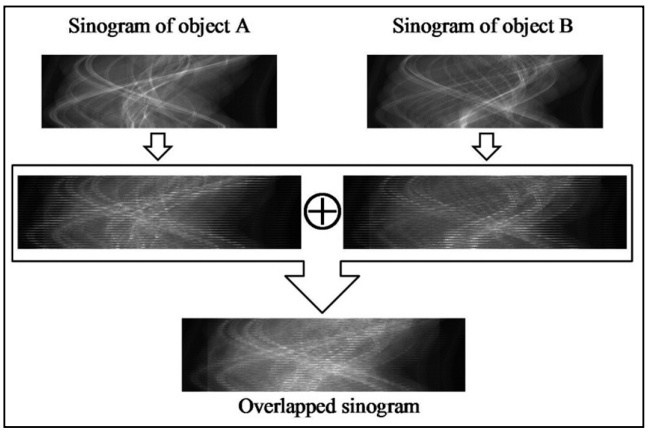

Fig. 5. Overlapped sinogram generated from two non-overlapped sinograms. First row: raw data collected at SSRF in the rotation mode only; second row: re-arranged data equivalent to that collected in the rotation-translation mode; third row: overlapped data to be used for reconstruction using our proposed approach.

where u_i stands for the displacement of the i^{th} object at the n^{th} view, H is the amplitude of the translation and T is the number of views between two translations. By construction, the objects' motion along vertical direction is restricted in the range $[-H, H]$. We should keep in mind that the effective width of the x-ray beam is relatively narrow, thus the value of H cannot be large. It is assumed that the value of H is relatively small, thus we only concentrate on certain positions on the translation, i.e. the positions at $u_i = -H$ and $u_i = H$ for two objects, and the positions at $u_i = -H$, $u_i = 0$ and $u_i = H$ for three objects, etc. After every T views, each object was translated to the next position. According to Eq. (6), each object occupies a unique position in one view. In Fig. 3, we show the sinogram of a single object in the rotation-translation mode, where the value of T is 2 so that the center of each projection line is changed after every 2 views.

For a better understanding of the system matrixes in this process, we will analyze two objects' case as an example. Here we introduce a zero matrix M_{exp}, the size of which is $W_3 \times W_4$, $W_3 = \left\lceil \frac{2H}{w_b} \right\rceil$, $W_4 = W_1 \cdot W_2$, where w_b is the distance between two bins on the detector array. From Eq. (6), the centers of the two objects are switched between $u_i = -H$ and $u_i = H$. Without loss of generality, let the first object's center be $u_1 = H$ at the n^{th} view, and denote the original system matrix as M (see Section 2.1). Then its system matrix can be expressed as $M_1 = \begin{bmatrix} M \\ M_{\text{exp}} \end{bmatrix}$, and the second object's system matrix is $M_2 = \begin{bmatrix} M_{\text{exp}} \\ M \end{bmatrix}$. The zero matrix M_{exp} in M_1 corresponds to the x-rays only passing through the second object.

By doing so, we get the system matrixes for those objects whose motion consisted of rotation and translation. They are unique for different objects. The remaining work becomes solving Eq. (4) using an appropriate algorithm. Because most of the projections are overlapped, the linear system described in Eq. (2) is still under-determined. Therefore, more constraints should be imposed to guarantee the uniqueness of the solution. Notice that the gradient images of our objects are quite sparse, that is, many elements are zeros or nearly zeros, we can minimize their l_1 norm (or total variation) as a penalty term to find the best solution.

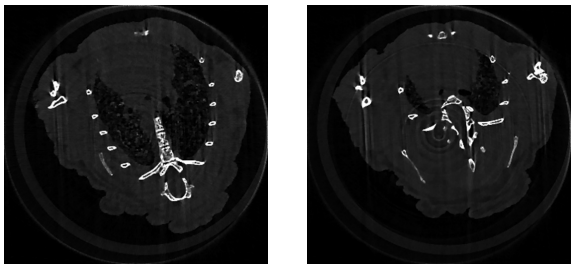

Fig. 6. Two images reconstructed from non-overlapped data.

2.4. *Efficiency analysis*

In the rotation-only scanning mode, objects are scanned in sequence, and the time cost is $t_1 = N_o n t_s$, where n is the number of views, and t_s the time for acquiring one single sinogram. In the rotation-translation mode, objects are scanned simultaneously, and it will take only $t_2 = nt_s + \left\lceil \frac{n}{T} \right\rceil t_\theta$, where t_θ is the time for each translation; see Fig. 4. The symbol η is used for efficiency, and defined as $\eta = \frac{t_2}{t_1} \approx \frac{1}{N}(1 + \frac{t_\theta}{T \cdot t_s})$. A smaller η means a higher efficiency. In micro-CT, acquiring a single sinogram usually takes 15$\sim$20 s (for x-ray exposure and data transfer), and in synchrotron CT it is $\sim$3 s. Assuming that t_θ <1 s (it is reasonable because the distance between two center positions can be relatively small), the value of η can be $\sim$54% in the case of two objects with $T = 4$, and $\sim$33% in the case of four objects with $T = 1$. That is, about half time is saved when scanning two objects simultaneously, and two-third time saved when scanning four objects simultaneously. Moreover, a phantom study in [15] indicated that the image quality of a single slower scan was better than a dual-rotation double-speed scan. Thus, we would suggest an exposure time longer than 3 s.

2.5. *SART-TV algorithm*

The reconstruction algorithm for the proposed scanning mode can be summarized in two major steps [3, 5]. First, a standard simultaneous algebraic reconstruction technique (SART) is used to reconstruct discrete images $\vec{f}_i (i = 1, 2, \ldots, N_o)$ from the overlapped projections. Second, the l_1 norm for a given sparse transform of the discrete images is minimized using the steepest descent method, i.e. the TV minimization step.

We define

$$M_i^{j,+} = \sum_{k=1}^{W_1 \cdot W_2} M_i^{j,k} \text{ for } j = 1, \ldots, N_b \tag{7}$$

$$M_i^{+,k} = \sum_{j=1}^{N_b} M_i^{j,k} \text{ for } k = 1, \ldots, W_1 \cdot W_2 \tag{8}$$

Where N_b is the number of bins on the detector array.

Then, for our problem the SART formula [16] is expressed as

$$f_i^{q+1}(k) = f_i^q(k) + \frac{1}{M_i^{+,k}} \sum_{j=1}^{N_b} \frac{M_i^{j,k}}{\sum_{k=1}^{N_o} M_k^{j,+}} [p(j) - \bar{p}^q(j)] \tag{9}$$

where $p(j)$ is the overlapped projection at j^{th} bin on the detector array, and $\bar{p}^q(j)$ is the calculated projection at q^{th} iteration.

The workflow of the algorithm is described in the following pseudo-code:

1 : Initialize the parameters: α, N_{grad}, $k = 0$, $\overrightarrow{f_i^0} = 0 (i = 1, 2, \ldots, N_o)$
2 : **Repeat the main loop** % SART reconstruction
3 : $q = q + 1$; $\overrightarrow{f_i^q} = \overrightarrow{f_i^{q-1}}$;
4 : Determine the system matrixes for each object according to Eq. (6);
5 : Update $\overrightarrow{f_i^q}$ by Eq. (9) from overlapped projections;
6 : Enforce the negative elements in $\overrightarrow{f_i^q}$ to be 0;
7 : Calculate the image differences between two iterations $D_i = \left\| \overrightarrow{f_i^q} - \overrightarrow{f_i^{q-1}} \right\|_2$;
8 : **For** $I_{grad} = 1$ **to** N_{grad} **do** % TV minimization
9 : Compute the steepest decent direction vector $\overrightarrow{d_i}$;
10: Normalize the vectors $\overrightarrow{d_i}$ to obtain $\widehat{d_i}$;
11: Update the image: $\overrightarrow{f_i^q} = \overrightarrow{f_i^q} - \alpha \cdot D_i \cdot \widehat{d_i}$;
12: **End for** (I_{grad})
13: **Until the stopping criteria are satisfied.**

As specified in line 1, the minimization of TV is controlled by the parameter α which affects image refinement in terms of the distance D_i, and N_{grad} is the total number of gradient descent steps to be performed each time. Lines 3–5 perform the reconstruction using the SART/OS-SART technique to update images $\overrightarrow{f_i}$ from overlapped projections, and non-negativity is enforced in line 6. Lines 8–11 define the sub-loop for TV minimization. Line 9 computes the steepest decent direction d_i of intermediate images. The magnitude of the gradient can be approximately expressed as

$$\mu_{m,n} \approx \sqrt{(f_{m,n} - f_{m-1,n})^2 + (f_{m,n} - f_{m,n-1})^2}. \tag{10}$$

TV can be defined as $\left\| \vec{f} \right\|_{TV} = \sum_m \sum_n \mu_{m,n}$. Then, the steepest descent direction is defined by

$$\begin{aligned} d_{m,n} &= \frac{\partial \left\| \overrightarrow{f} \right\|_{TV}}{\partial f_{m,n}} \\ &\approx \frac{(f_{m,n} - f_{m-1,n}) + (f_{m,n} - f_{m,n-1})}{\mu_{m,n} + \varepsilon} - \frac{(f_{m+1,n} - f_{m,n})}{\mu_{m+1,n} + \varepsilon} - \frac{(f_{m,n+1} - f_{m,n})}{\mu_{m,n+1} + \varepsilon}. \end{aligned} \tag{11}$$

In Eq. (11), we have ignored the subscript index i of images, and included a small positive number ε in the denominator to avoid any singularity. The iteration stopped when there is no appreciable change in the intermediate images. Other stopping criteria may include the maximum number of iterations, total variation of the image, and other image quality indexes. Here we prefer the steepest descent method for its simplicity and effectiveness. If the system matrix becomes larger, the computational efficiency will be a critical problem. In such a situation, a first-order compressed sensing approach as proposed by Choi et al. [17], or a GPU-based acceleration technique as proposed by Jia et al. [18] would be very useful.

Table 1
PSNR (dB) of reconstructed images with fixed T = 1

	H = 0.87 mm	H = 1.74 mm	H = 3.48 mm	H = 6.96 mm
Object A	27.9710	28.0605	28.3713	28.8670
Object B	29.0402	28.5490	28.8485	29.3530

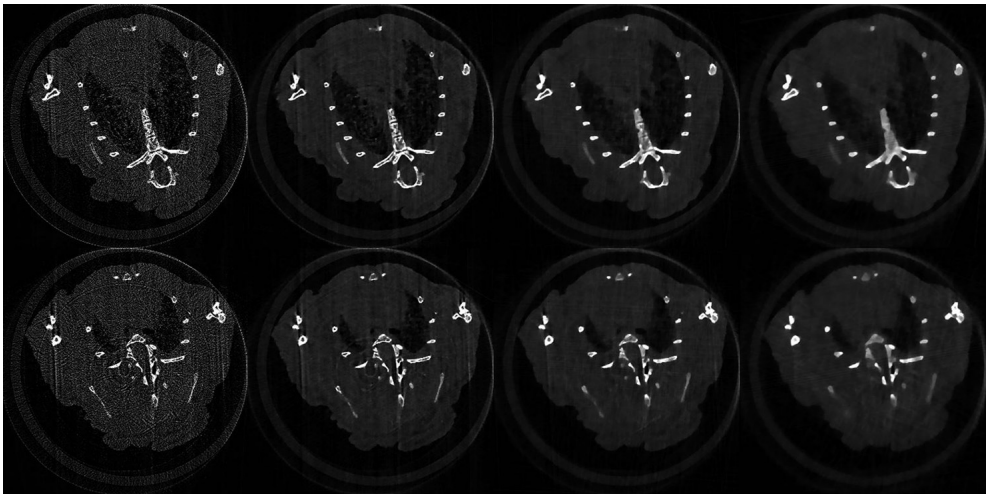

Fig. 7. Effects of the TV term. From left to right are the images reconstructed with $\alpha = 0$, 0.05, 0.1 and 0.2, respectively.

3. Numerical results

In this section, we report a number of studies in the cases of two and four objects respectively. The raw data of mice was collected at Shanghai Synchrotron Radiation Facility (SSRF). In this preliminary evaluation, we used numerical method to generate overlapped projections equivalent to those obtained in the rotation-translation mode; see Fig. 5. We first scanned four mice separately in the rotation mode only, then rearranged the center position of each projection line according to Eq. (6), and finally added the re-arranged sinograms to obtain overlapped data. In Subsections 3.1 and 3.2, we adjusted the values of α, H and T to show their effects on the reconstructed images. In Subsection 3.3, we describe simultaneously scanned and reconstructed four objects.

The support of each mouse was 25×25 mm^2. The detector array consisted of 805 bins over 35 mm. The reconstructed images were of 350×350 pixels. Each mouse was scanned with 230 views uniformly distributed over a 180° range. The images reconstructed from non-overlapped sinograms served as the standard for comparison; see Fig. 6.

3.1. Effects of TV

The process of the total variation minimization was controlled by two parameters, the iteration number N_{grad} for gradient descent steps and the step size α. Here, we fixed $N_{grad} = 2$ and changed the value of α from 0 to 0.2. The object motion was described by Eq. (6) with $T = 1$ and $H = 3.5$ mm. The reconstruction process was stopped after 4600 iterations. From Fig. 7 the value of α around 0.05 had the best performance. When α was larger than 0.1, the images became too smooth to show structural details. Therefore, the TV term was fixed at $\alpha = 0.05$ and $N_{grad} = 2$ in the subsequent tests.

Table 2
PSNR(dB) of reconstructed images with fixed H = 3.48 mm

	T = 1	T = 4	T = 16	T = 32
Object A	28.3713	28.2338	27.8933	27.6629
Object B	28.8485	28.5477	28.5369	27.6190

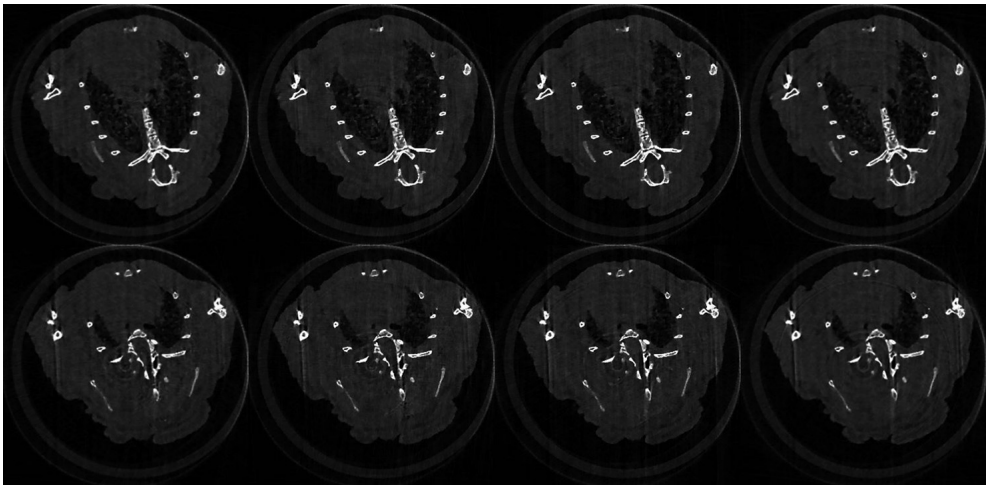

Fig. 8. Reconstructed images of two objects with different H values in the rotation-translation mode. From left to right the values of H are 0.87 mm, 1.74 mm, 3.48 mm and 6.96 mm, respectively. The value of T is always 1.

3.2. Effects of H and T

In the proposed rotation-translation mode, except rotation the objects are also translating in a sequence of positions given by Eq. (6). Such position is determined by two factors, T and H. We assumed that the value of H is quite small, hence the detector can receive all projections and the time cost for each translation is comparable to that for the data acquisition process at each view. To verify the correctness of this assumption, we performed four reconstructions with different values of H, i.e. 0.87 mm, 1.74 mm, 3.48 mm and 6.96 mm. The value of T was fixed at 1, which meant the positions of two objects were switched every view. For each reconstruction the number of main iterations was 4600 together with 2 sub-iterations for TV minimization. The results were displayed in Fig. 8. It was quite clear that if the objects switched their positions at a high rate (or equivalently a small number of T), the images can be well reconstructed even the value of H was under 2.5% of the detector's length. When we increased the value of H, there were no visible changes in the reconstructed images. For comparison, we fixed H at 3.48 mm (approximately 10% of the detector's length) and examined what would happen if the value of T was increased. In Fig. 9, the image quality remained good only when the value of T was relatively small, and severe artifacts appeared when T became quite large. The reconstructed images were evaluated using peak-to-peak signal-to-noise ratio (PSNR). The bigger the value of PSNR, the better the reconstructed images. The results were displayed in Tables 1 and 2. The ground true images were reconstructed using filtered backprojection algorithm with non-overlapped 1150 projections.

3.3. Simultaneous reconstruction of four objects

In the last experiment, two more objects were added. The values of T and H were made 1 and 5.22 mm,respectively. Hence, the loci of the object center points were

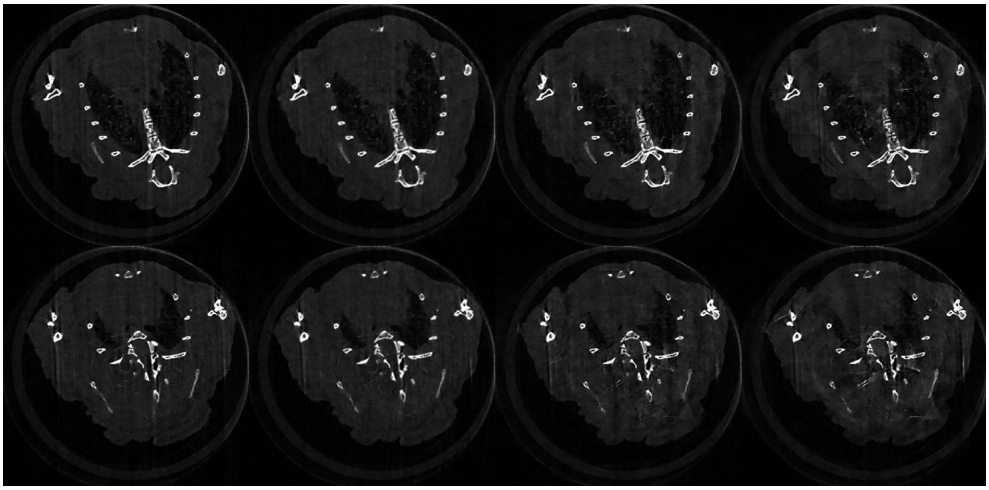

Fig. 9. Reconstructed images of two objects with different T in the rotation-translation mode. From left to right the values of T are 1, 4, 16 and 32, respectively. The value of H is always 3.48 mm.

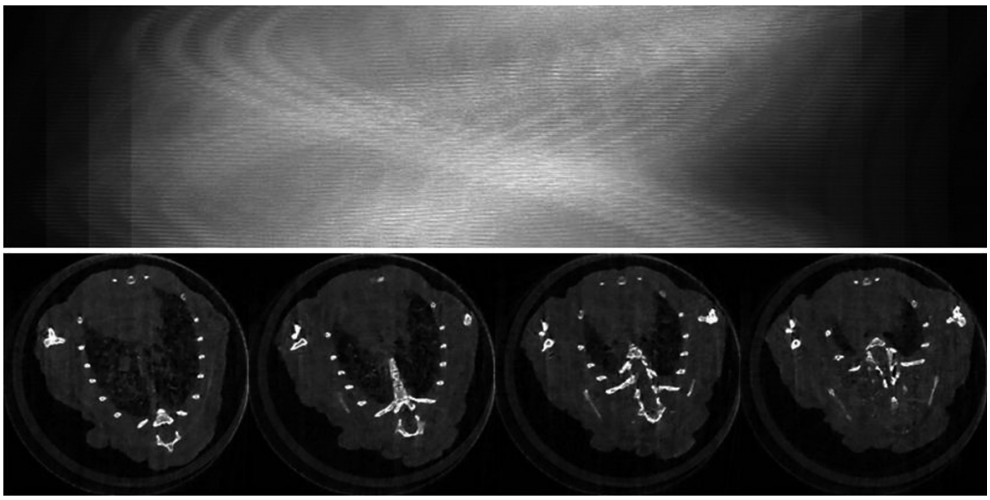

Fig. 10. Top: the sinogram of four objects in the rotation-translation scanning mode with $H = 5.22\ mm$ and $T = 1$; bottom: the reconstructed images.

$$u_1 := \left\{ \frac{H}{3}, H, -H, -\frac{H}{3}, \ldots, \right\}$$

$$u_2 := \left\{ H, -H, -\frac{H}{3}, \frac{H}{3}, \ldots, \right\}$$

$$u_3 := \left\{ -H, -\frac{H}{3}, \frac{H}{3}, H, \ldots, \right\}$$

$$u_4 := \left\{ -\frac{H}{3}, \frac{H}{3}, H, -H, \ldots, \right\}$$

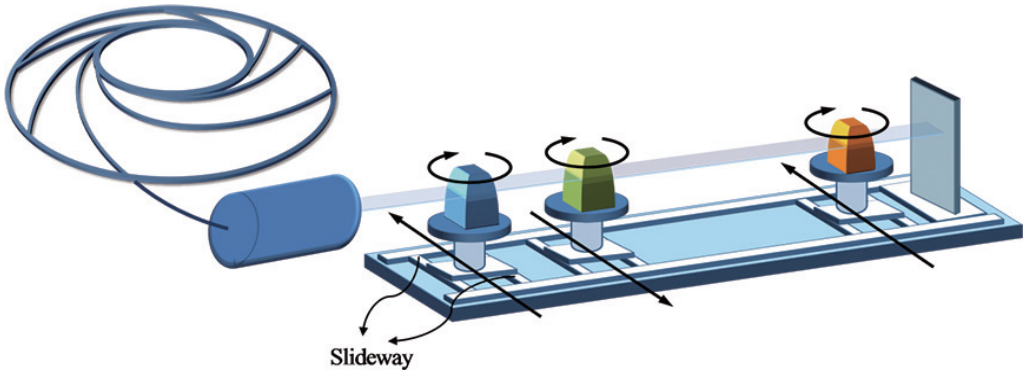

Fig. 11. Experimental settings for the proposed mode using the beamline BL13W of SSRF. (Colours are visible in the online version of the article; http://dx.doi.org/10.3233/XST-2012-0337)

Other parameters remained the same as what we had used in the case of two objects. The results are in Fig. 10. Although we successfully separated those objects and the main structures such as bones were very clear, the image quality was not as good as that in the case of two objects. Due to the highly overlapped nature of projection data (two times more than that of two objects), there were slightly more interferences among the images.

4. Discussions and conclusion

The reconstruction of multiple objects is very attractive in the synchrotron radiation facilities, since it makes full use of the high energy x-rays and can reduce time. Fast and reliable results are especially important for those experiments need to scan a large number of samples regularly. The overlapped projections contain abundant information. With some prior knowledge, the performance of the overlapped projections is comparable to that by the individual projections. In our new scanning mode, the translation was introduced to make the system matrixes for each object different. In real applications, this can be achieved using two motors for each sample stage. The values of T and H determine the object loci. Since the sparsity of the image varies case by case, there is no fixed T or H. In our context, it has been suggested to choose $T \leqslant 4$ for two objects and $T = 1$ for four objects. The value of H is flexible depending on the object support and the detector size. Simply increasing the value of H will not solve our problem, but a large H will definitely improve the image quality since many projections are not overlapped. Let us consider an extreme case that the value of H is larger than the half length of the detector so that all the projections are not overlapped. Then the problem becomes to that of solving two independent reconstruction problems. Reconstruction of more than four objects was not recommended using the current approach. As discussed in Subsection 2.4, in this new mode the scanning efficiency will be 2$\sim$3 times higher than before. The proposed method is specifically designed for the scenario where a large number of samples need to be scanned using a synchrotron CT facility. It is for screening samples. If the sample contains many complicated or interesting structures, we would perform a second scan with a higher quality protocol.

Our new scanning mode is especially designed for Shanghai Synchrotron Radiation Facility (SSRF), which is a third-generation synchrotron radiation light source and the largest imaging platform for research and development in China. The energy of the storage ring is 3.5 GeV, which is the highest

among the medium-energy light sources. The beamline BL13W of SSRF is designed for x-ray biomedical applications. Figure 11 shows the experimental settings for the proposed mode in SSRF in the future.

In conclusion, we have investigated the feasibility of simultaneously reconstructing multiple objects from overlapped projections. A rotation-translation scanning mode has been proposed and evaluated with promising results. In reference to recent CS-based methods [19–21], further efforts are needed to implement and refine our method for important biological or preclinical applications using the Shanghai Synchrotron Radiation Facility (SSRF).

Acknowledgement

This work was supported in part by the National Basic Research Program of China (2010CB834300), the National Science Foundation of China (30570511 and 30770589), the National High Technology Research and Development Program of China (2007AA02Z452), and the National Science Foundation of USA (NSF/CMMI 0923297).

References

[1] C.A. Carlsson, Imaging modalities in x-ray computerized tomography and in selected volume tomography, *Physics in Medicine and Biology* **44** (1999), R23.
[2] A. Del Guerra, N. Belcari, G.L. Llacer, S. Marcatili, S. Moehrs and D. Panetta, Advanced radiation measurement techniques in diagnostic radiology and molecular imaging, *Radiation Protection Dosimetry* **131** (2008), 136.
[3] H. Yu and G. Wang, Compressed sensing based interior tomography, *Physics in Medicine and Biology* **54** (2009), 2791.
[4] E.Y. Sidky, C.M. Kao and X. Pan, Accurate image reconstruction from few-views and limited-angle data in divergent-beam CT, *Journal of X-Ray Science and Technology* **14** (2006), 119–139.
[5] G.H. Chen, J. Tang and S. Leng, Prior image constrained compressed sensing (PICCS): A method to accurately reconstruct dynamic CT images from highly undersampled projection data sets, *Medical Physics* **35** (2008), 660.
[6] Y. Lin, Y. Lu and G. Wang, Compressed sensing inspired image reconstruction from overlapped projections, *International Journal of Biomedical Imaging* **2010** (2010).
[7] D.L. Donoho, Compressed sensing, *Information Theory, IEEE Transactions on* **52** (2006), 1289–1306.
[8] Y. Tsaig and D.L. Donoho, Extensions of compressed sensing, *Signal Processing* **86** (2006), 549–571.
[9] M.F. Duarte, M.A. Davenport, D. Takhar, J.N. Laska, T. Sun, K.F. Kelly and R.G. Baraniuk, Single-pixel imaging via compressive sampling, *Signal Processing Magazine, IEEE* **25** (2008), 83–91.
[10] M. Mishali and Y.C. Eldar, Blind multiband signal reconstruction: Compressed sensing for analog signals, Signal Processing, *IEEE Transactions on* **57** (2009), 993–1009.
[11] M. Lustig, D. Donoho and J.M. Pauly, Sparse MRI: The application of compressed sensing for rapid MR imaging, *Magnetic Resonance in Medicine* **58** (2007), 1182–1195.
[12] D.J. Brady, K. Choi, D.L. Marks, R. Horisaki and S. Lim, Compressive holography, *Optics Express* **17** (2009), 13040–13049.
[13] R.L. Siddon, Fast calculation of the exact radiological path for a three-dimensional CT array, *Medical Physics* **12** (1985), 252.
[14] H. Yu, C. Ji and G. Wang, SART-Type image reconstruction from overlapped projections, *International Journal of Biomedical Imaging* **2011** (2010).
[15] T. Li and L. Xing, Optimizing 4D cone-beam CT acquisition protocol for external beam radiotherapy, *International Journal of Radiation Oncology Biology Physics* **67** (2007), 1211–1219.
[16] M. Jiang and G. Wang, Convergence of the simultaneous algebraic reconstruction technique (SART), *Image Processing, IEEE Transactions on* **12** (2003), 957–961.
[17] K. Choi, J. Wang, L. Zhu, T.S. Suh, S. Boyd and L. Xing, Compressed sensing based cone-beam computed tomography reconstruction with a first-order method, *Medical Physics* **37** (2010), 5113.
[18] X. Jia, Y. Lou, J. Lewis, R. Li, X. Gu, C. Men, W.Y. Song and S.B. Jiang, GPU-based fast low-dose cone beam CT reconstruction via total variation, *Journal of X-Ray Science and Technology* **19** (2011), 139–154.
[19] L. Jacques, A short note on compressed sensing with partially known signal support, *Signal Processing* **90** (2010), 3308–3312.

[20] K. Qiu and A. Dogandzic, Variance-component based sparse signal reconstruction and model selection, *Signal Processing, IEEE Transactions on* **58** (2010), 2935–2952.
[21] W. Guo and W. Yin, Edgecs: Edge guided compressive sensing reconstruction, *Rice CAAM Report TR10* **2** (2010), 30.